Journal of Solid State Chemistry **158,** 290–298 (2001)
doi:10.1006/jssc.2001.9109, available online at http://www.idealibrary.com on IDEAL®

Structural Characterization of New Layered Perovskites MLa$_2$Ti$_2$TaO$_{10}$ (M = Cs, Rb) and NaLa$_2$Ti$_2$TaO$_{10}$ · xH$_2$O (x = 2, 0.9, 0)

Young-Sik Hong, Chi-Hwan Han, and Keon Kim

Division of Chemistry and Molecular Engineering, Department of Chemistry, Korea University, Seoul 136-701, Korea
E-mail: youngsikh@yahoo.com

Received October 24, 2000; in revised form January 2, 2001; accepted January 19, 2001; published online April 5, 2001

The crystal structures of $n = 3$ Dion–Jacobson phases MLa$_2$Ti$_2$TaO$_{10}$ (M = Cs, Rb) and NaLa$_2$Ti$_2$TaO$_{10}$ · xH$_2$O (x = 2, 0.9, 0) have been investigated by the Rietveld analysis of their powder XRD patterns. These compounds show the new-type ordering sequence of (Ti$_{1/2}$Ta$_{1/2}$)O$_6$–TiO$_6$–(Ti$_{1/2}$Ta$_{1/2}$)O$_6$ in the tripled octahedra, corresponding to the niobium analogs of MLa$_2$Ti$_2$NbO$_{10}$. They crystallize in the tetragonal system $P4/mmm$ with lattice constants of a = 3.84733(9) and c = 15.4364(4) Å for CsLa$_2$Ti$_2$TaO$_{10}$, and a = 3.8342(2) and c = 15.2776(9) Å for RbLa$_2$Ti$_2$TaO$_{10}$. Sodium-exchanged phase was easily hydrated to NaLa$_2$Ti$_2$TaO$_{10}$ · 2H$_2$O, belonging to the space group $I4/mmm$ with a = 3.8399(3) and c = 34.288(3) Å. Upon firing, NaLa$_2$Ti$_2$TaO$_{10}$ · 2H$_2$O was dehydrated to NaLa$_2$Ti$_2$TaO$_{10}$ · 0.9H$_2$O with $P4/mmm$ at around 100°C and then NaLa$_2$Ti$_2$TaO$_{10}$ with $I4/mmm$ at above 200°C. The Na cations in two hydrates were surrounded with six oxygens, forming face-shared octahedra along (110) direction. These structural models, especially for the coordination environment of Na cations, were proposed for the first time. © 2001 Academic Press

Key Words: **layered perovskite; Dion–Jacobson phase; hydrate; ordering.**

INTRODUCTION

Over 20 years, an intensive research has been carried out in the area of layered perovskite compounds based on perovskite-structured $A_{n-1}B_nO_{3n+1}$ layers, which are separated by large metal cations or metal oxides along one of the perovskite cubic directions. Aurivillius phases $(Bi_2O_2)A_{n-1}B_nO_{3n+1}$, Ruddlesden–Popper phases $M_2A_{n-1}B_nO_{3n+1}$ (R-P phases) and Dion–Jacobson phases $MA_{n-1}B_nO_{3n+1}$ (D-J phases) are well known examples (1–3). Among them, two series of R-P and D-J phases exhibit a variety of chemical properties such as ion-exchange and intercalation reactions (4, 5). Especially ion-exchangeable layered perovskites made up of NbO_6, TiO_6, or TaO_6 octahedra have gained interest, because of their two-dimensional (2-D) physical properties, such as catalysis, ionic conductivity, and luminescence.

Recently, many groups are trying to develop the various synthetic routes of metastable solids by the combination of high-temperature solid-state and soft-chemical reactions. For instance, Bhuvanesh *et al.* have synthesized new 3-D perovskites through the dehydration reaction of R-P phases $H_2A_{0.5n}B_nO_{3n+1} \cdot xH_2O$ (A = Ca, Sr; B = Nb, Ta) (6). In addition, Aurivillius and R-P phases could be interchanged by the selective leaching of Bi_2O_2 sheet and metathesis reaction (7, 8). Schaak and Mallouk have prepared an A-site ordered 3-D perovskite, $CaEu_2Ti_3O_9$, from $n = 3$ R-P phase $Na_2Eu_2Ti_3O_{10}$ (9). Very recently, we have demonstrated that the B-site cations in $CsLn_2Ti_2NbO_{10}$ (Ln = La, Pr, Nd, Sm) are arranged into the new-type ordering sequence of $(Ti_{1/2}Nb_{1/2})O_6$–TiO_6–$(Ti_{1/2}Nb_{1/2})O_6$ (10). These results indicate that various metastable 3-D perovskites with specific sequence of A- and/or B-site cations can be prepared by the reduction, dehydration, and ion-exchange reactions of 2-D layered perovskites.

In this paper, we report the structural characterization of new layered titanotantalates, MLa$_2$Ti$_2$TaO$_{10}$ (M = Cs, Rb) and NaLa$_2$Ti$_2$TaO$_{10}$ · xH$_2$O. The structural models for the new hydrates NaLa$_2$Ti$_2$TaO$_{10}$ · xH$_2$O (x = 2, 0.9) are also proposed.

EXPERIMENTAL

2-D layered perovskites, MLa$_2$Ti$_2$TaO$_{10}$, were prepared by conventional solid-state reaction of M_2CO_3 (Aldrich, 99.9%), La_2O_3 (Aldrich, 99.9%), TiO_2 (Aldrich, 99%), and Ta_2O_5 (Aldrich, 99.5%). Excess amounts of M_2CO_3 (25 mol%) were added to compensate for loss due to the volatilization of the alkali metal components. The reactants were ball-milled in ethanol for 12 h and then calcined at 1100°C for 2 days in alumina crucibles. After the reaction, the obtained products were washed with distilled water. The sodium-exchanged phase was obtained by heating 0.5 g of CsLa$_2$Ti$_2$TaO$_{10}$ in molten NaNO$_3$ at 400°C for 2 days. The obtained product was thoroughly washed with distilled water. The completeness of each ion-exchange reaction was

0022-4596/01 $35.00

estimated by energy-dispersive X-ray emission (EDX) analysis and powder X-ray diffraction (XRD) method.

EDX analysis of $M\mathrm{La_2Ti_2TaO_{10}}$ gave a stoichiometric composition within experimental errors. Powder XRD data of the samples were collected with a MACMXP powder diffractometer at room temperature and a Philips X'pert MPD attached high temperature furnace, with Cu$K\alpha$ radiation. Step scans were performed over the angular range $10^\circ < 2\theta < 100^\circ$ with the step size of 0.026° and the counting time of 3 s. The compounds were refined by the Rietveld method using the Fullprof program (11). The peak shape was described by a pseudo-Voigt function. The background level was defined by a polynomial function. For each diffraction pattern, the scale factor, the counter zero point, the peak asymmetry, and the unit-cell dimensions were refined in addition to the atomic parameters. Thermogravimetic analysis (TGA, Dupont SDT 2960) was performed on the sodium phase. Samples of about 30 mg were placed in an alumina crucible and heated at a heating rate of 5°C/min in air.

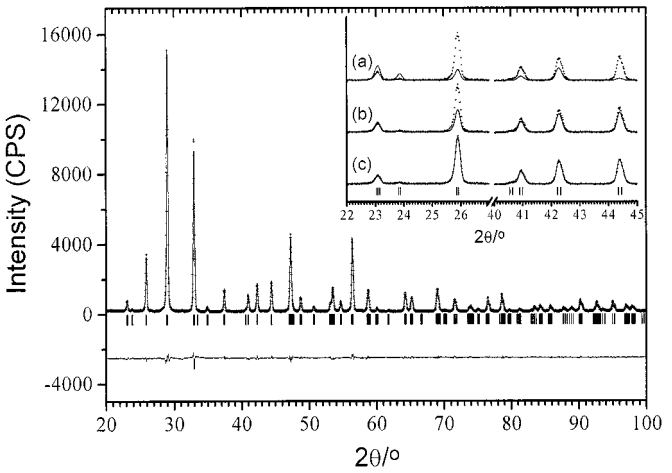

FIG. 1. Observed, calculated, and difference powder XRD profiles of $\mathrm{CsLa_2Ti_2TaO_{10}}$, using space group $P4/mmm$. Selected observed and calculated powder XRD profiles refined by the arrangement of (a) $\mathrm{TiO_6}$–$\mathrm{TaO_6}$–$\mathrm{TiO_6}$, (b) $(\mathrm{Ti_{2/3}Ta_{1/3}})\mathrm{O_6}$–$(\mathrm{Ti_{2/3}Ta_{1/3}})\mathrm{O_6}$–$(\mathrm{Ti_{2/3}Ta_{1/3}})\mathrm{O_6}$, and (c) $(\mathrm{Ti_{1/2}Ta_{1/2}})\mathrm{O_6}$–$\mathrm{TiO_6}$–$(\mathrm{Ti_{1/2}Ta_{1/2}})\mathrm{O_6}$ are shown in the inset.

RESULTS

$MLa_2Ti_2TaO_{10}$ (M = Cs, Rb)

All peaks of XRD patterns could be indexed on the tetragonal system $P4/mmm$ with $a = 3.84733(9)$ and $c = 15.4364(4)$ Å. The observed, calculated, and difference powder XRD profiles of $\mathrm{CsLa_2Ti_2TaO_{10}}$ are presented in Fig. 1. As previously stated in Ref. (10), the Ti^{4+} and Ta^{5+} cations can be distributed over two crystallographically independent sites; $2g$ (0, 0, ~0.28) and $1a$ (0, 0, 0). More profitably, the larger difference of atomic scattering power of Ti^{4+} and Ta^{5+} in $\mathrm{CsLa_2Ti_2TaO_{10}}$ would be helpful to refine the B-site cation arrangement than in $\mathrm{CsLa_2Ti_2TaO_{10}}$. At the first stage, the refinement was carried out using the arrangement of $\mathrm{TiO_6}$–$\mathrm{TaO_6}$–$\mathrm{TiO_6}$, and it gave the agreement factors of $R_p = 40.6\%$, $R_{wp} = 46.6\%$, and $R_I = 31.1\%$ (Fig. 1a). The arrangement of $(\mathrm{Ti_{2/3}Ta_{1/3}})\mathrm{O_6}$–$(\mathrm{Ti_{2/3}Ta_{1/3}})\mathrm{O_6}$–$(\mathrm{Ti_{2/3}Ta_{1/3}})\mathrm{O_6}$ was adopted to improve the fit, but all the agreement factors of $R_p = 18.2\%$, $R_{wp} = 21.1\%$, and $R_I = 12.5\%$ were still high (Fig. 1b). The equal amounts of Ti^{4+} and Ta^{5+} cations are located at $2g$ sites and only Ti^{4+} cations at $1a$, resulting in the arrangement of $(\mathrm{Ti_{1/2}Ta_{1/2}})\mathrm{O_6}$–$\mathrm{TiO_6}$–$(\mathrm{Ti_{1/2}Ta_{1/2}})\mathrm{O_6}$. Then the refinement gave the good agreement factors of $R_p = 10.6\%$, $R_{wp} = 11.6\%$, and $R_I = 3.23\%$. Finally, the site occupancies of Cs^+, La^{3+}, Ti^{4+}, and Ta^{5+} cations were refined, but no significant deviation was found. Consequently, it can be demonstrated that the distribution of B-site cations in tripled octahedra shows the new-type ordering sequence of $(\mathrm{Ti_{1/2}Ta_{1/2}})\mathrm{O_6}$–$\mathrm{TiO_6}$–$(\mathrm{Ti_{1/2}Ta_{1/2}})\mathrm{O_6}$ within an acceptable error limit. In the same way, the above sequence was applied to refine the XRD pattern of $\mathrm{RbLa_2Ti_2TaO_{10}}$ with space group $P4/mmm$. The refined atomic positions, isotropic thermal parameters, and bond distances of $\mathrm{CsLa_2Ti_2TaO_{10}}$ and $\mathrm{RbLa_2Ti_2TaO_{10}}$ are listed in Tables 1 and 2.

Thermal Stability of $NaLa_2Ti_2TaO_{10}\cdot 2H_2O$

EDX analysis indicated that most (ca. 95%) of the Cs^+ cations in $\mathrm{CsLa_2Ti_2TaO_{10}}$ were exchanged by Na^+ cations in $\mathrm{NaNO_3}$ melts. The obtained Na phase was strongly hygroscopic upon exposure to the atmosphere. The TG and d(TG)/d(Temp) curves of $\mathrm{NaLa_2Ti_2TaO_{10}}\cdot x\mathrm{H_2O}$ are presented in Fig. 2. The total weight loss at the temperature ranges of 25–300°C corresponds to the two $\mathrm{H_2O}$ molecules. As can be seen in the TG and d(TG)/d(Temp) curves, the following dehydration reactions take place through two successive steps: $\mathrm{NaLa_2Ti_2TaO_{10}}\cdot 2\mathrm{H_2O} \rightarrow \mathrm{NaLa_2Ti_2TaO_{10}}\cdot 0.9\mathrm{H_2O} + 1.1\mathrm{H_2O}$ (↑) $\rightarrow \mathrm{NaLa_2Ti_2TaO_{10}} + 0.9\mathrm{H_2O}$(↑). The measurements of the powder XRD patterns of $\mathrm{NaLa_2Ti_2TaO_{10}}\cdot x\mathrm{H_2O}$ were carried out *in situ* by the X-ray diffractometer with high-temperature furnace attachment, as shown in Fig. 3. The main (103) reflection peak of $\mathrm{NaLa_2Ti_2TaO_{10}}\cdot 2\mathrm{H_2O}$ disappeared at around 100°C, and the new (103) reflection peak of $\mathrm{NaLa_2Ti_2TaO_{10}}\cdot 0.9\mathrm{H_2O}$ can be detected at $2\theta = 28.9^\circ$. On the other hand, the characteristic reflections of the perovskite sublattice (110) and (200) keep their original positions all over the temperature ranges, indicating the retention of perovskite-like $\mathrm{La_2Ti_2TaO_{10}}$ slabs along the ab plane. These TG and XRD results indicate that the new phase $\mathrm{NaLa_2Ti_2TaO_{10}}\cdot 0.9\mathrm{H_2O}$ exists around at 100°C. Above 200°C, the (107) reflection peak of anhydrous phase $\mathrm{NaLa_2Ti_2TaO_{10}}$ could be observed, keeping their (110) and (200) reflections.

TABLE 1
Crystallographic Data of $M La_2Ti_2TaO_{10}$ and $M La_2Ti_2TaO_{10} \cdot xH_2O$

	Atom	Site	g	x	y	z	B_{iso}(Å^2)
$CsLa_2Ti_2TaO_{10}$	Cs	1*d*	1	$\frac{1}{2}$	$\frac{1}{2}$	$\frac{1}{2}$	1.85(8)
	La	2*h*	1	$\frac{1}{2}$	$\frac{1}{2}$	0.1408(1)	0.35(6)
$a = 3.84733(9)$ Å	Ti	1*a*	1	0	0	0	0.58(6)
$c = 15.4364(4)$ Å	Ti/Ta(2)	2*g*	1	0	0	0.2829(1)	0.58(6)
$R_p = 10.1\%$	O(1)	4*n*	0.5	0.109(5)	$\frac{1}{2}$	0	1.3(5)
$R_{wp} = 11.1\%$	O(2)	2*g*	1	0	0	0.1197(7)	1.3(5)
$R_I = 2.83\%$	O(3)	4*i*	1	0	$\frac{1}{2}$	0.2500(6)	1.3(5)
	O(4)	2*g*	1	0	0	0.3943(7)	1.3(5)
$RbLa_2Ti_2TaO_{10}$	Rb	1*d*	1	$\frac{1}{2}$	$\frac{1}{2}$	$\frac{1}{2}$	2.9(2)
	La	2*h*	1	$\frac{1}{2}$	$\frac{1}{2}$	0.1435(2)	0.42(9)
$a = 3.8342(2)$ Å	Ti(1)	1*a*	1	0	0	0	0.9(1)
$c = 15.2776(9)$ Å	Ti/Ta(2)	2*g*	1	0	0	0.2889(2)	0.9(1)
$R_p = 13.7\%$	O(1)	4*n*	0.5	0.113(5)	$\frac{1}{2}$	0	1.5(2)
$R_{wp} = 14.8\%$	O(2)	2*g*	1	0	0	0.1206(9)	1.5(2)
$R_I = 4.19\%$	O(3)	4*i*	1	0	$\frac{1}{2}$	0.2557(8)	1.5(2)
	O(4)	2*g*	1	0	0	0.4034(12)	1.5(2)
$NaLa_2Ti_2TaO_{10} \cdot 2H_2O$	Na	8*g*	0.25	0	$\frac{1}{2}$	0.2845(9)	0.5(1)
	La	4*e*	1	0	0	0.43642(6)	0.5(1)
	Ti(1)	2*a*	1	0	0	0	0.9(1)
$a = 3.8399(3)$ Å	Ti/Ta(2)	4*e*	1	0	0	0.12754(8)	0.9(1)
$c = 34.288(3)$ Å	O(1)	8*j*	0.5	0.088(7)	$\frac{1}{2}$	0	1.3(2)
$R_p = 15.4\%$	O(2)	4*e*	1	0	0	0.0546(6)	1.3(2)
$R_{wp} = 17.7\%$	O(3)	8*g*	1	0	$\frac{1}{2}$	0.1139(4)	1.3(2)
$R_I = 5.93\%$	O(4)	4*e*	1	0	0	0.1804(6)	1.3(2)
	Ow	4*e*	0.99	0	0	0.2734(5)	1.3(2)
$NaLa_2Ti_2TaO_{10} \cdot 0.9H_2O$	Na	2*e*	0.5	$\frac{1}{2}$	0	$\frac{1}{2}$	0.7(2)
	La	2*h*	1	$\frac{1}{2}$	$\frac{1}{2}$	0.1449(9)	0.7(2)
	Ti(1)	1*a*	1	0	0	0	0.7(2)
$a = 3.8408(6)$ Å	Ti/Ta(2)	2*g*	0.5	0	0	0.2820(5)	0.7(2)
$c = 15.510(3)$ Å	O(1)	4*n*	0.5	0.09(2)	$\frac{1}{2}$	0	1.2(4)
$R_p = 19.4\%$	O(2)	2*g*	1	0	0	0.121(2)	1.2(4)
$R_{wp} = 22.7\%$	O(3)	4*i*	1	0	$\frac{1}{2}$	0.254(3)	1.2(4)
$R_I = 5.53\%$	O(4)	2*g*	1	0	0	0.398(5)	1.2(4)
	Ow	1*d*	0.90	$\frac{1}{2}$	$\frac{1}{2}$	$\frac{1}{2}$	1.2(4)
$NaLa_2Ti_2TaO_{10}$	Na	4*d*	0.5	0	$\frac{1}{2}$	$\frac{1}{4}$	0.5(1)
$a = 3.8356(3)$ Å	La	4*e*	1	0	0	0.4267(1)	0.5(1)
$c = 29.733(2)$ Å	Ti(1)	2*a*	1	0	0	0	0.5(1)
	Ti/Ta(2)	4*e*	0.5	0	0	0.1475(2)	0.5(1)
$R_p = 20.2\%$	O(1)	8*j*	0.5	0.121(8)	$\frac{1}{2}$	0	0.7(3)
$R_{wp} = 17.9\%$	O(2)	4*e*	1	0	0	0.0614(6)	0.7(3)
$R_I = 5.79\%$	O(3)	8*g*	1	0	$\frac{1}{2}$	0.1332(5)	0.7(3)
	O(4)	4*e*	1	0	0	0.2077(9)	0.7(3)

$NaLa_2Ti_2TaO_{10} \cdot 2H_2O$

The observed, calculated, and difference powder XRD profiles of $NaLa_2Ti_2TaO_{10} \cdot 2H_2O$ are shown in Fig. 4. The most reliable solutions with physically meaningful parameters were achieved by adopting the atomic parameters of $NaCa_2Ta_3O_{10}$ ($a = 3.8607$ and $c = 29.216$ Å) with the space group *I*4/*mmm* (12). One different point is that the *c* lattice constant of $NaLa_2Ti_2TaO_{10} \cdot 2H_2O$ is much larger than that of $NaCa_2Ta_3O_{10}$, even though the ionic size of Ti^{4+} is smaller than that of Ta^{5+}. This means that the H_2O molecules were intercalated into the interlayer, similar to the $n = 2$ D-J hydrate $NaLaTa_2O_7 \cdot 1.90H_2O$ (13). However, the structure was successfully refined by positioning the Na cations and H_2O molecules (only oxygen atom was assigned) in 8*g* and 4*e* sites, in contrast to 4*e* and 8*g* sites in $NaLaTa_2O_7 \cdot 1.90H_2O$. The occupation factor of H_2O molecules was adopted as the value obtained by TG analysis. This setting gave the agreement factors of $R_p = 15.4\%$, $R_{wp} = 17.7\%$, and $R_I = 5.93\%$.

TABLE 2
Selected Bond Distances of $M La_2Ti_2TaO_{10}$ and $M La_2Ti_2TaO_{10} \cdot xH_2O$

	$CsLa_2Ti_2TaO_{10}$	$RbLa_2Ti_2TaO_{10}$	$NaLa_2Ti_2TaO_{10} \cdot 2H_2O$	$NaLa_2Ti_2TaO_{10} \cdot 0.9H_2O$	$NaLa_2Ti_2TaO_{10}$
A–O(4)	8 × 3.172(6)	8 × 3.087(9)	2 × 2.190(19)	4 × 2.492(20)	4 × 2.294(20)
A–Ow			2 × 2.841(33)		
A–Ow			2 × 1.973(11)	2 × 1.920(15)	
La–O(1)	2 × 3.198(8)	2 × 3.215(8)	2 × 3.136(18)	2 × 3.034(18)	2 × 3.230(18)
La–O(1)	2 × 2.642(9)	2 × 2.647(7)	2 × 2.695(14)	2 × 2.882(14)	2 × 2.620(14)
La–O(2)	4 × 2.740(1)	4 × 2.734(2)	4 × 2.733(2)	4 × 2.741(2)	4 × 2.735(2)
La–O(3)	4 × 2.557(6)	4 × 2.572(8)	4 × 2.582(11)	4 × 2.557(11)	4 × 2.616(11)
Ti(1)–O(1)	4 × 1.969(9)	4 × 1.966(7)	4 × 1.976(6)	4 × 1.924(6)	4 × 1.973(6)
Ti(1)–O(2)	2 × 1.847(8)	2 × 1.843(8)	2 × 1.812(18)	2 × 1.877(18)	2 × 1.827(18)
Ti/Ta(2)–O(2)	1 × 2.520(9)	1 × 2.571(9)	1 × 2.502(19)	1 × 2.297(19)	1 × 2.560(19)
Ti/Ta(2)–O(3)	4 × 1.990(2)	4 × 1.983(2)	4 × 1.949(4)	4 × 1.970(4)	4 × 1.965(4)
Ti/Ta(2)–O(4)	1 × 1.721(9)	1 × 1.750(9)	1 × 1.870(24)	1 × 1.794(24)	1 × 1.788(24)
Ow–O(4)			1 × 3.189(27)		
Ow–O(4)			4 × 3.145(12)		
Ow–Ow			4 × 3.153(13)		

$NaLa_2Ti_2TaO_{10} \cdot 0.9H_2O$

The observed, calculated, and difference powder XRD profiles of $NaLa_2Ti_2TaO_{10} \cdot 0.9H_2O$ are presented in Fig. 5. All peaks of XRD patterns obtained at 100°C were indexed on the tetragonal cell $P4/mmm$ with $a = 3.8484(7)$ and $c = 15.499(4)$ Å. These lattice constants are comparable to those of $CsLa_2Ti_2TaO_{10}$, indicating that H_2O molecules are positioned in the Cs site. The refinement was carried out using a three-phase model, because of the presence of significant amounts of $NaLa_2Ti_2TaO_{10} \cdot 2H_2O$ and $NaLa_2Ti_2TaO_{10}$. The Na cations and H_2O molecules were positioned in the $2e$ ($\frac{1}{2}$, 0, $\frac{1}{2}$) and $1d$ ($\frac{1}{2}$, $\frac{1}{2}$, $\frac{1}{2}$) sites, which gave the somewhat high agreement factors of $R_p = 19.4\%$, $R_{wp} = 22.7\%$, and $R_I = 5.53\%$ due to the poor crystallinity. The relative percentages were refined to 16% $NaLa_2Ti_2TaO_{10} \cdot 2H_2O$, 74% $NaLa_2Ti_2TaO_{10} \cdot 0.9H_2O$, and 10% $NaLa_2Ti_2TaO_{10}$.

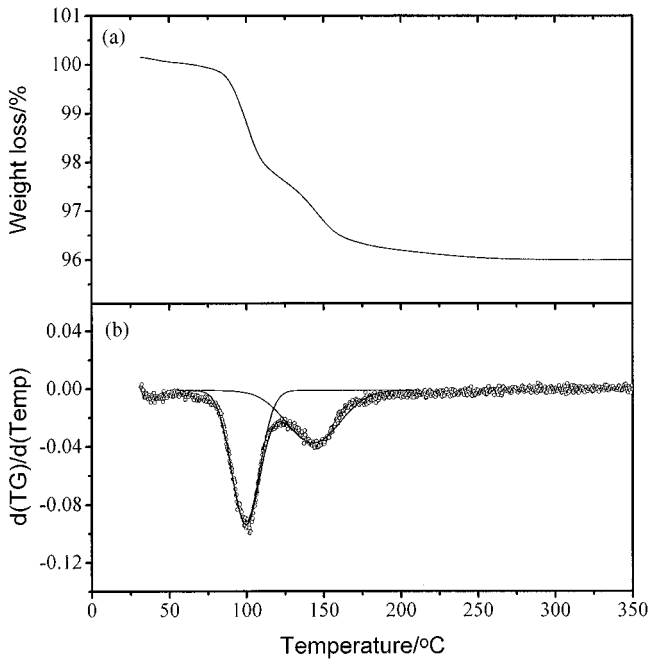

FIG. 2. Thermal behavior of $NaLa_2Ti_2TaO_{10} \cdot 2H_2O$. (a) TG and (b) d(TG)/d(Temp.)

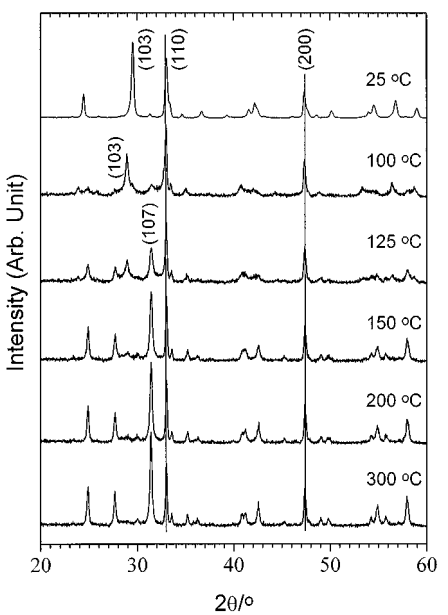

FIG. 3. Powder XRD patterns of $NaLa_2Ti_2TaO_{10} \cdot 2H_2O$ recorded at temperatures from room temperature to 300°C.

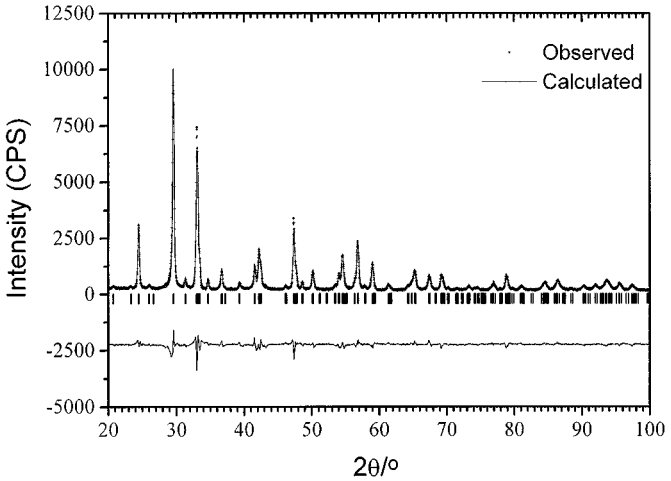

FIG. 4. Observed, calculated, and difference powder XRD profiles of $NaLa_2Ti_2TaO_{10} \cdot 2H_2O$.

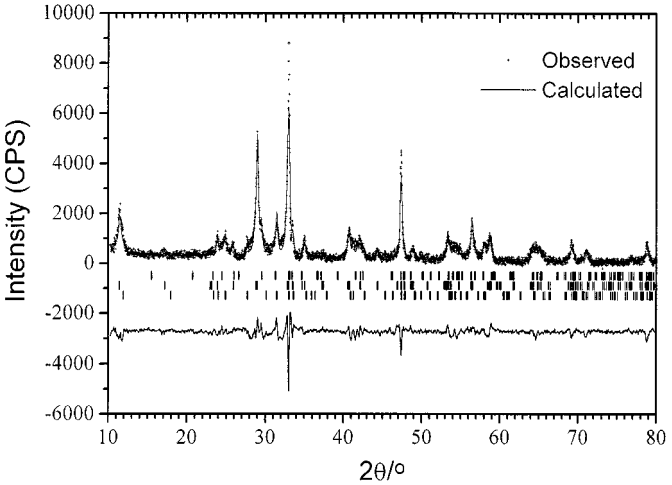

FIG. 5. Observed, calculated, and difference powder XRD profiles of $NaLa_2Ti_2TaO_{10} \cdot 0.9H_2O$. Top tick, $NaLa_2Ti_2TaO_{10} \cdot 2H_2O$; middle tick, $NaLa_2Ti_2TaO_{10} \cdot 0.9H_2O$, and bottom tick, $NaLa_2Ti_2TaO_{10}$.

$NaLa_2Ti_2TaO_{10}$

The observed, calculated, and difference powder XRD profiles of $NaLa_2Ti_2TaO_{10}$ obtained at 300°C are presented in Fig. 6. It was refined by the structure parameter using the space group $I4/mmm$ (12). The occupation factor of Na cations was kept to 0.5 at 4*d* sites during the refinement. The refined atomic positions, isotropic thermal parameters, and bond distances of $NaLa_2Ti_2TaO_{10} \cdot xH_2O$ ($x = 2, 0.9, 0$) are also listed in Tables 1 and 2. The successive transformations from $CsLa_2Ti_2TaO_{10}$ to $NaLa_2Ti_2TaO_{10}$ are presented in Fig. 7.

DISCUSSION

B-Site Cation Arrangement

The ordering behavior of the B-site cations in 3-D perovskites $A(B', B'')O_3$ depends on the magnitude of the size and charge differences between B' and B'' cations. In this regard, it is worthy to note that the new-type ordering sequence of B-site cations, for the first time, is found in $n = 3$ D-J phases $MLa_2Ti_2BO_{10}$ (B = Ta, Nb), even though the size and charge differences are not significant at all. As discussed in Ref. (10), it could be considered $CsLa_2Ti_2TaO_{10}$ as the intergrowths of CsO rock salt and $La_2Ti_2TaO_9$ perovskite layers. Then, $CsLa_2Ti_2TaO_{10}$ can be simply cut out as the chain of $[CsO]^{-1}$–$[La_{1/2}(Ti_{1-x}Ta_x)O_3]^{x-0.5}$–$[La(Ti_{2x}Ta_{1-2x})O_3]^{-2x+2}$–$[La_{1/2}(Ti_{1-x}Ta_x)O_3]^{x-0.5}$–$[CsO]^{-1}$, depending on the distribution of B-site cations. Assuming that $x = 0.5$, it gives the arrangement with charge distribution of $[CsO]^{-1}$–$[La_{1/2}(Ti_{1/2}Ta_{1/2})O_3]^0$–$[LaTiO_3]^{+1}$–$[La_{1/2}(Ti_{1/2}Ta_{1/2})O_3]^0$–$[CsO]^{-1}$. This means that the electrostatic stabilization by the insertion of $[CsO]^{-1}$ layer into 3-D perovskite structure may contribute to the new-type ordering of Ti^{4+}/Ta^{5+} and Ti^{4+} cations along z-axis, confirmed by the Madelung lattice energy calculation (10). Based on the bond character of octahedra, Gopalakrishnan *et al.* had argued that the arrangement of B-site cations in $CsLa_2Ti_2NbO_{10}$ would be NbO_6–TiO_6–NbO_6, corresponding to $x = 0$ (14). However, it shows the unfavorable charge distribution of $[CsO]^{-1}$–$[La_{1/2}TiO_3]^{-0.5}$–$[LaNbO_3]^{+2}$–$[La_{1/2}TiO_3]^{-0.5}$–$[CsO]^{-1}$, giving rise to the electrostatic repulsion between $[CsO]^{-1}$ and $[La_{1/2}TiO_3]^{-0.5}$.

Besides this ordering behavior, there is a possibility of tilting or rotation of BO_6 octahedra, suggested by the displacements in O(1) sites [ideal position $2f$ $(0, \frac{1}{2}, 0)$] in $MLa_2Ti_2TaO_{10}$. An acceptable temperature factor was

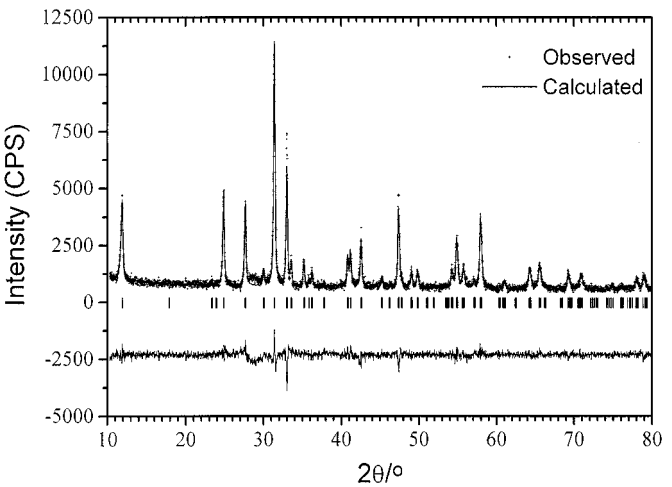

FIG. 6. Observed, calculated, and difference powder XRD profiles of $NaLa_2Ti_2TaO_{10}$.

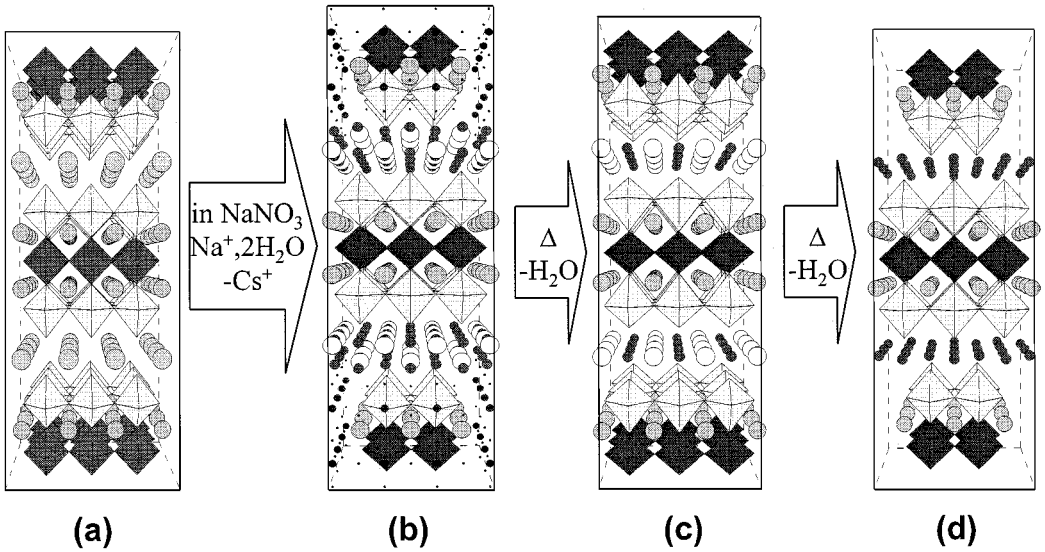

FIG. 7. Crystal structures and schematic transformations. (a) $CsLa_2Ti_2TaO_{10}$, (b)$NaLa_2Ti_2TaO_{10}\cdot 2H_2O$, (c) $NaLa_2Ti_2TaO_{10}\cdot 0.9H_2O$, and (d) $NaLa_2Ti_2TaO_{10}$. Open octahedra, $(Ti_{1/2}Ta_{1/2})O_6$; solid octahedra, TiO_6; small solid circles, Na; large open circles, Cs/H_2O; and large solid circles; La. All crystallographic sites were fully occupied and the O(1) sites were positioned in ideal sites.

obtained only by allowing relaxation off the $\langle 100\rangle$ mirror plane to two half-occupied 4*n* sites, as observed in $n = 3$ R-P phase $NaLa_2Ti_3O_{10}$ (15). Such a distortion is typically observed when the A cation is too small for the cubic BO_3 corner-sharing octahedral network. In such cases the *A*–O distances can be softened by the distortion of octahedra while the first coordination sphere around the *B* cation remains unchanged. In fact, a large number of extra peaks were observed in $CsLnTi_2NbO_{10}$ (*Ln* = Pr, Nd, Sm, Eu), suggesting the lowering of crystal symmetry from *P*4/*mmm* to *Pnam* as decreasing the A-site cation size, as shown in $CsCa_2Nb_3O_{10}$ (16). Although we cannot preclude the possible existence of short-range ordering due to tilting or rotation in $CsLaTi_2TaO_{10}$, no superstructure reflections were apparent in the XRD profile of $CsLaTi_2TaO_{10}$.

Then, what about the R-P and Aurivillius phases? According to Schaak and Mallouk, they have prepared $n = 3$ R-P phase $K_2SrLaTi_2TaO_{10}$ by solid-state reaction method (17). In the similar way, $K_2SrLaTi_2TaO_{10}$ can be thought as the intergrowths of K_2O and $SrLaTi_2TaO_9$ perovskite layers, made of $[K_2O]^0$–$[(Sr_{1/4}La_{1/4})(Ti_{1-x}Ta_x)O_3]^{x-0.75}$–$[(Sr_{1/2}La_{1/2})(Ti_{2x}Ta_{1-2x})O_3]^{-2x+1.5}$–$[(Sr_{1/4}La_{1/4})(Ti_{1-x}Ta_x)O_3]^{x-0.75}$–$[K_2O]^0$. This gives a charge separation of [0]–[−]–[+]–[−]–[0] for all *x* ranges. In this case, an advantageous attractive effect of [−]–[+]–[−] would be offset by the repulsive effect of [−]–[0]–[−]. This means that the electrostatic interaction would not be a dominant factor for the B-site cation arrangements. Actually, it was reported that the Ti^{4+} and Ta^{5+} cations in $K_2SrLaTi_2TaO_{10}\cdot 2H_2O$ were statistically distributed in the tripled octahedra. To be lacking in $K_2SrLaTi_2TaO_{10}\cdot 2H_2O$, it was not single-phase compound. Thus, we have tried to investigate other single-phase compounds such as $Na_2(Ca,Sr)LaTi_2NbO_{10}$, but there was the other problem that the large cations of Na, Ca(Sr), and La could be occupied in the interlayer and/or perovskite A sites, as shown in the compounds such as $Na_2La_2Ti_3O_{10}$, $(Ca,Sr)_4Ti_3O_{10}$, and $La_4Ni_3O_{10}$.

To further confirm this concept, we have also synthesized Aurivillius phases such as $(Bi_2O_2)BiPbTi_2NbO_{10}$ and $(BiPbO_2)La_2Ti_2NbO_{10}$. Likewise, these phases can be regarded as the chains of Bi_2O_3 and perovskite layers, $[Bi_2O_3]^0$–$[(Bi_{1/4}Pb_{1/4})(Ti_{1-x}Nb_x)O_3]^{x-0.75}$–$[(Bi_{1/2}Pb_{1/2})(Ti_{2x}Ta_{1-2x})O_3]^{-2x+1.5}$–$[(Bi_{1/4}Pb_{1/4})(Ti_{1-x}Ta_x)O_3]^{x-0.75}$–$[Bi_2O_3]^0$ for $(Bi_2O_2)BiPbTi_2NbO_{10}$ and $[BiPbO_3]^{-1}$–$[La_{1/2}(Ti_{1-x}Ta_x)O_3]^{x-0.5}$–$[La(Ti_{2x}Ta_{1-2x})\ O_3]^{-2x+2}$–$[La_{1/2}(Ti_{1-x}Ta_x)O_3]^{x-0.5}$–$[BiPbO_3]^{-1}$ for $(BiPbO_2)La_2Ti_2NbO_{10}$. In this regard, both compounds have the charge distribution similar with $K_2SrLaTi_2TaO_{10}$ and $CsLaTi_2TaO_{10}$, respectively. According to the results of preliminary refinement, $(Bi_2O_2)BiPbTi_2NbO_{10}$ shows the random sequence of $(Ti_{0.64}Nb_{0.36})O_6$–$(Ti_{0.72}Nb_{0.28})O_6$–$(Ti_{0.64}Nb_{0.36})O_6$, while $(BiPbO_2)La_2Ti_2NbO_{10}$ exhibits $(Ti_{0.56}Nb_{0.44})O_6$–$(Ti_{0.88}Nb_{0.12})O_6$–$(Ti_{0.56}Nb_{0.44})O_6$ near the new-type ordering sequence. These facts support that the concept of building block can be viewed as a new idea to understand the B-site cation arrangement of layered perovskites. A further study is required to confirm this because of the possibility of the cation mixing of Bi and Pb as $Na_2(Ca,Sr)LaTi_2NbO_{10}$ (18). The neutron diffraction studies on R-P and Aurivillius phases are in progress.

Environment of Na Cations in $NaLa_2Ti_2TaO_{10}\cdot 2H_2O$

For the 2-D layered hydrates, Toda *et al.* has characterized some layered perovskites, such as 3 R-P and $n = 2$ D-J phases (12, 13). Even Schaak and Mallouk also gave the lattice constants of $a = 3.7971(3)$ and $c = 34.067(5)$ Å for $NaEu_2Ti_2NbO_{10}\cdot xH_2O$, but no reports for the crystal structure of $n = 3$ D-J hydrates were addressed (9). We could only find that the study on the crystal structure of $NaCa_2Ta_3O_{10}\cdot xH_2O$ is in progress (19). Concerning the local environments of Na cations, the structure of $NaLa_2Ti_2TaO_{10}\cdot 2H_2O$ is different from those of $NaLaTa_2O_7\cdot 1.90H_2O$ ($n = 2$ D-J phase) and $K_2La_2Ti_3O_{10}\cdot 2H_2O$ ($n = 3$ R-P phase). The Na cations in $NaLaTa_2O_7\cdot 1.90H_2O$ are surrounded by four oxygens belonging to the outer octahedra and four oxygens of H_2O molecules in 8*g* sites, resulting in a tetragonal prismatic coordination (13). Although it is difficult to determine the accurate positions of Na cations and H_2O molecules owing to their smaller contributions to the structure factors, their positional information can be inferred from the structural viewpoint. Considering that their positions are exchangeable over the two 8*g* and 4*e* sites in *I*4/*mmm*, $Na_4^{8g}La_2^{4e}[Ti_2Ta]^{4e/2a}O_{10}\cdot 2H_2O^{4e}$ and $Na_4^{4e}La_2^{4e}[Ti_2Ta]^{4e/2a}O_{10}\cdot 4H_2O^{8g}$ would be given to fully occupied compositions. This means that the occupation factors should be cut down to 25% Na in the former and 50% Na and 50% H_2O in the latter to give the experimental composition of $NaLa_2Ti_2TaO_{10}\cdot 2H_2O$. We can examine the interlayer of Na cations and H_2O molecules to visualize how this manifests itself within the structure. Let's try to remove them by assuming that all the vacancies are ordered in a special manner along (110) direction, where they are deleted by the solid and dashed lines, as shown in Figs. 8a and 8b. Consequently, in $Na^{8g}La_2^{4e}[Ti_2Ta]^{4e/2a}O_{10}\cdot 2H_2O^{4e}$ the Na cations are bonded to four oxygens of H_2O and two oxygens of outer octahedra, producing face-shared octahedral arrangements (Fig. 8c). On the contrary, in $Na^{4e}La_2^{4e}[Ti_2Ta]^{4e/2a}O_{10}\cdot 2H_2O^{8g}$ the Na cations are bonded to four oxygens of H_2O and four oxygens of outer octahedra, forming a tetragonal antiprismatic anti coordination (Fig. 8d). These models could be indirectly examined by thermal stability of H_2O molecules in $NaLa_2Ti_2TaO_{10}\cdot 2H_2O$, where two H_2O molecules were dehydrated at the different temperature ranges, as shown in Fig. 3. Additionally, the Na cations in 8*g* sites allow two kinds of H_2O with short and

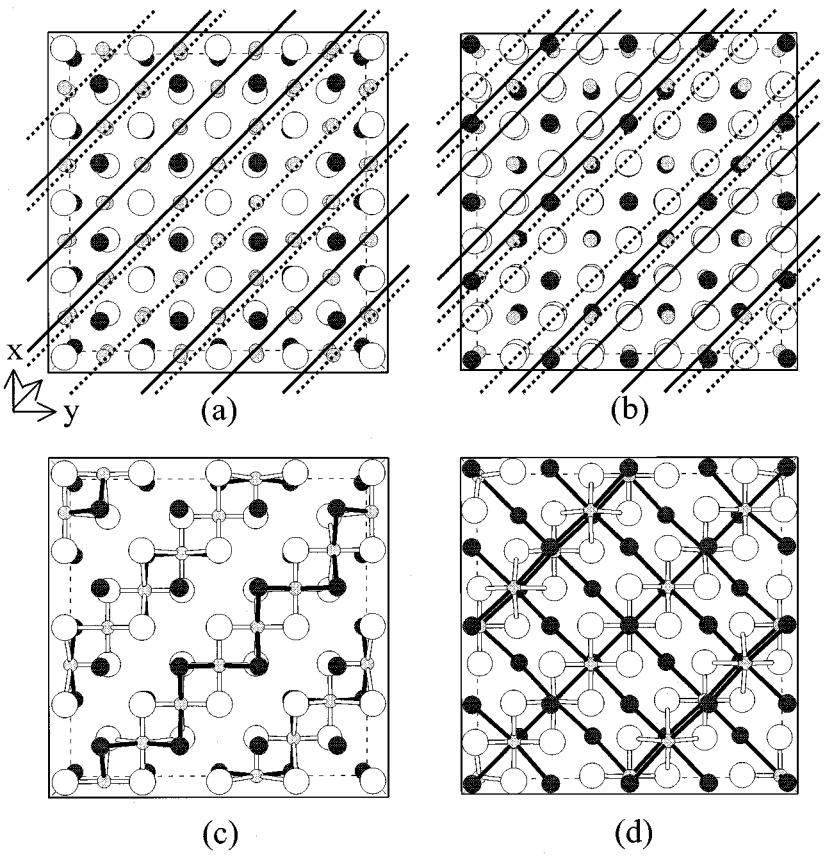

FIG. 8. Proposed local environment of Na cations in $NaLa_2Ti_2TaO_{10}\cdot 2H_2O$. (a) $Na_4^{8g}La_2^{4e}[Ti_2Ta]^{4e/2a}O_{10}\cdot 2H_2O^{4e}$, (b) $Na_2^{4e}La_2^{4e}[Ti_2Ta]^{4e/2a}O_{10}\cdot 4H_2O^{8g}$, (c) $Na^{8g}La_2^{4e}[Ti_2Ta]^{4e/2a}O_{10}\cdot 2H_2O^{4e}$, and (d) $Na^{4e}La_2^{4e}[Ti_2Ta]^{4e/2a}O_{10}\cdot 2H_2O^{8g}$. Large open circles, H_2O molecules; small solid circles, O(4); and small gray circles, Na.

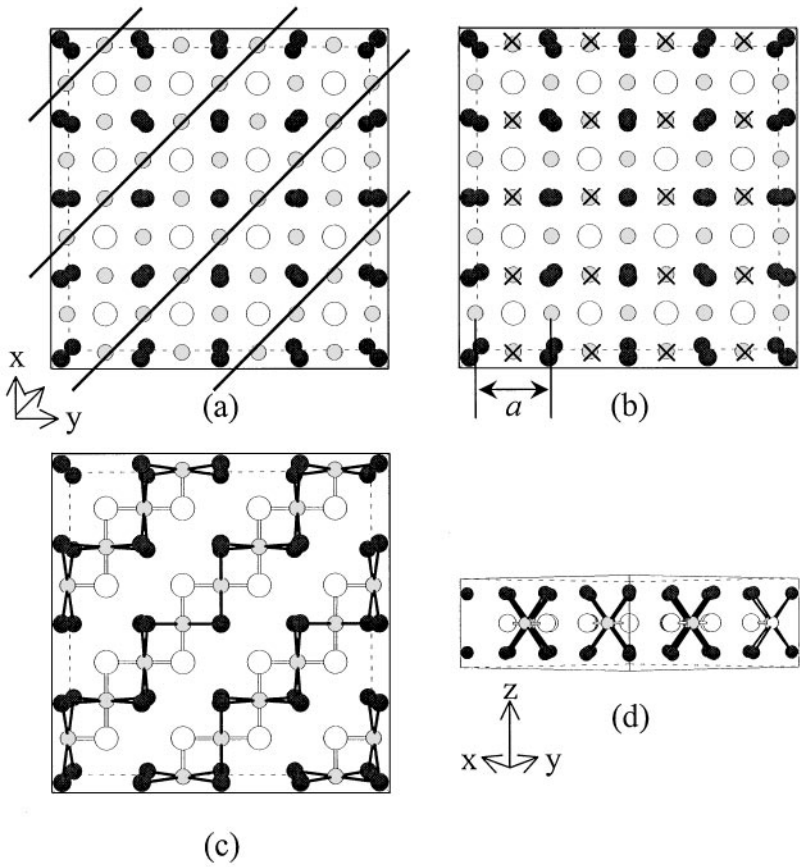

FIG. 9. Proposed local environment of Na cations in $NaLa_2Ti_2TaO_{10}\cdot 0.90H_2O$. Extraction along (a) (110) and (b) (100) directions in $Na_2^{2e}La_2^{2e}[Ti_2Ta]^{2g/1a}O_{10}\cdot H_2O^{1h}$, (c) $Na^{2e}La_2^{2e}[Ti_2Ta]^{2g/1a}O_{10}\cdot H_2O^{1h}$, and (d) $Na^{2e}La_2^{2e}[Ti_2Ta]^{2g/1a}O_{10}\cdot H_2O^{1h}$ viewed along z axis. Large open circles, H_2O molecules; small solid circles, O(4); and small gray circles, Na.

long Na–Ow bond distances (Table 2), while the Na cations in 4*e* sites gives only four Na–Ow bonds with same bond distances. Therefore, it can be concluded that the structural model of $Na^{8g}La_2^{4e}[Ti_2Ta]^{4e/2a}O_{10}\cdot 2H_2O^{4e}$ is more acceptable than that of $Na^{4e}La_2^{4e}[Ti_2Ta]^{4e/2a}O_{10}\cdot 2H_2O^{8g}$. The similar TG results were observed in $NaLn_2Ti_2NbO_{10}\cdot xH_2O$ (Y.-S. Hong and K. Kim, accepted in *Mater. Res. Bull.*).

Environment of Na Ions in $NaLa_2Ti_2TaO_{10}\cdot 0.9H_2O$ and $NaLa_2Ti_2TaO_{10}$

The local environment of Na cations in $NaLa_2Ti_2TaO_{10}\cdot 0.9H_2O$ can be also suggested by considering their structural requirements. Assuming that 2*e* and 1*d* sites in *P*4/*mmm* are fully occupied, the composition would be given to $Na_2^{2e}La_2^{2e}[Ti_2Ta]^{2g/1a}O_{10}\cdot H_2O^{1h}$, as shown in Fig. 9. This indicates that the occupation factor of Na cations should be cut down to 50% to give the experimental composition of $NaLa_2Ti_2TaO_{10}\cdot 0.9H_2O$. Then, the vacancies should be created along (110) direction, because the sum (4.84 Å) of ionic radius of Na cations and oxygen in H_2O is larger than that of *a* unit cell parameter (3.82 Å) along (100) direction. In this vacancy ordering, the Na cations are bonded to two H_2O and four oxygens of outer octahedra, producing face-shared octahedral arrangements, similar to the structural behavior of $NaLa_2Ti_2TaO_{10}\cdot 2H_2O$. It is worthy to mention that there exist only two Na–Ow bond distances of 2.492 Å, as listed in Table 2. From these results, it may be thought that the formation of octahedral coordination around the Na cations is a driving force for the hydration of sodium-exchanged $n = 3$ D-J phases. For the anhydrous $NaLa_2Ti_2TaO_{10}$, the interlayer Na cations are located in the tetrahedral sites coordinated by four terminal oxygens, corresponding to the α-type $NaCa_2Nb_3O_{10}$ (20).

CONCLUSION

We have synthesized a series of new $n = 3$ D-J phases of $MLa_2Ti_2TaO_{10}$ (M = Cs, Rb) and $NaLa_2Ti_2TaO_{10}\cdot xH_2O$ ($x = 2$, 0.9, 0) with the new type ordering sequence of $(Ti_{1/2}Ta_{1/2})O_6$–TiO_6–$(Ti_{1/2}Ta_{1/2})O_6$. The ordering behavior in $n = 3$ D-J phases should be viewed consideration of

the electrostatic effect of the interlayer $[MO]^{-1}$, besides the size and charge differences. The crystal structure models for two hydrates were proposed for the first time. The local environments of Na cations were situated at 8*g* sites for $NaLa_2Ti_2TaO_{10} \cdot 2H_2O$ and 2*e* sites $NaLa_2Ti_2TaO_{10} \cdot 0.9H_2O$, forming face-shared octahedra along (110) direction. Although it is difficult to identify accurately the crystal structures of the two hydrates, owing to the smaller scattering power of Na cations and H_2O molecules, the thermal behavior and bond distances of the hydrates supported the proposed structural models. Therefore, one should keep in mind that the results obtained here on the atomic positions may be considered as a structural model rather than an accurate structure. Nonetheless, these structural models would provide a new concept on the crystal structure of hydrates such as D-J and R-P phases.

ACKNOWLEDGMENT

We gratefully acknowledge the support for this work by the Ministry of Education (BK21).

REFERENCES

1. B. Aurivillius, *Ark. Kemi* **2,** 519 (1950).
2. S. N. Ruddlesden and P. Popper, *Acta Crystallogr.* **10,** 538 (1957).
3. M. Dion, M. Ganne, and M. Tournoux, *Mater. Res. Bull.* **16,** 1429 (1981).
4. J. Gopalkrishnan and V. Bhat, *Inorg. Chem.* **26,** 4301 (1987).
5. T. Takata, Y. Furumi, K. Shinohara, A. Tanaka, M. Hara, J. N. Kondo, and K. Domen, *Chem. Mater.* **9,** 1063 (1997).
6. N. S. P. Bhuvanesh, M. P. Crosnier-Lopez, H. Duroy, and J. L. Fourquet, *J. Mater. Chem.* **10,** 1685 (2000).
7. W. Sugimoto, M. Shirata, Y. Sugahara, and K. Kuroda, *J. Am. Chem. Soc.* **121,** 11601 (1999).
8. J. Gopalakrishnan, T. Shivakumar, K. Ramesha, V. Thangadurai, and G. N. Subbanna, *J. Am. Chem. Soc.* **122,** 6237 (2000).
9. R. E. Schaak and T. E. Mallouk, *J. Am. Chem. Soc.* **122,** 2798 (2000).
10. Y.-S. Hong, S.-J. Kim, S.-J. Kim, and J.-H. Choy, *J. Mater. Chem.* **10,** 1209 (2000).
11. J. Rodriguez-Carvajal, Fullprof, version 3.2, January 1997, LLB.
12. K. Toda, T. Teranishi, Z.-G. Ye, M. Sato, and Y. Hinastu, *Solid State Ionics* **34,** 971 (1999).
13. K. Toda, K. Uematsu, and M. Sato, *J. Ceram. Soc. Jpn.* **105,** 482 (1997).
14. J. Gopalakrishnan, S. Uma, and V. Bhat, *Chem. Mater.* **5,** 132 (1993).
15. A. J. Wright and G. Greaves, *J. Mater. Chem.* **6,** 1823 (1996).
16. M. Dion, M. Ganne, and M. Tournoux, *Rev. Chim. Minér.* **21,** 92 (1984).
17. R. E. Schaak and T. E. Mallouk, *J. Solid State Chem.* **155,** 46 (2000).
18. C. H. Hervoches and P. Lightfoot, *J. Solid State Chem.* **153,** 66 (2000).
19. K. Toda, J. Watanabe, and M. Sato, *Mater. Res. Bull.* **31,** 1427 (1996).
20. H. Fukuoka, T. Isami, and S. Yamanaka, *Solid State Ionics* **151,** 40 (2000).